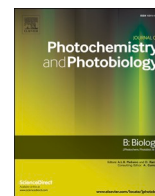




Contents lists available at ScienceDirect

Journal of Photochemistry & Photobiology, B: Biology

journal homepage: www.elsevier.com/locate/jphotobiolTowards *in vivo* photomediated delivery of anticancer peptides: Insights from pharmacokinetic and -dynamic data

Igor V. Komarov^{a,b,c,*}, Ganna Tolstanova^a, Halyna Kuznietsova^{a,c}, Natalia Dziubenko^a, Petro I. Yanchuk^a, Lydia Y. Shtanova^a, Stanislav P. Veselsky^a, Liudmyla V. Garmanchuk^a, Nataliia Khranovska^d, Oleksandr Gorbach^d, Taisa Dovbynchuk^a, Petro Borysko^c, Oleg Babii^{b,e}, Tim Schober^{b,e}, Anne S. Ulrich^{e,f,**}, Sergii Afonin^{e,***}

^a Taras Shevchenko National University of Kyiv, Kyiv, Ukraine^b Lumobiotics, Karlsruhe, Germany^c Enamine, Kyiv, Ukraine^d National Cancer Institute, Kyiv, Ukraine^e Karlsruhe Institute of Technology, Karlsruhe, Germany^f Institute of Organic Chemistry of Karlsruhe KIT, Fritz-Haber-Weg 6, 76131 Karlsruhe, Germany.

ARTICLE INFO

Keywords:

Anticancer peptides
Hepatocellular carcinoma
Molecular photoswitches
Pharmacokinetics
Pharmacodynamics
Photopharmacology

ABSTRACT

An *in vivo* study of a photoswitchable cytotoxic peptide LMB040 has been undertaken on a chemically induced hepatocellular carcinoma model in immunocompetent rats. We analysed the pharmacokinetic profile of the less toxic photoform ("ring-closed" dithienylethene) of the compound in tumors, plasma, and healthy liver. Accordingly, the peptide can reach a tumor concentration sufficiently high to exert a cytotoxic effect upon photoconversion into the more active ("ring-open") photoform. Tissue morphology, histology, redox state of the liver, and hepatic biochemical parameters in blood serum were analysed upon treatment with (i) the less active photoform, (ii) the *in vivo* light-activated alternative photoform, and (iii) compared with a reference chemotherapeutic 5-fluorouracil. We found that application of the less toxic form followed by a delayed *in vivo* photoconversion into the more toxic ring-open form of LMB040 led to a higher overall survival of the animals, and signs of enhanced immune response were observed compared to the untreated animals.

1. Introduction

Natural and artificial biologically active peptides are steadily making their way from scientific laboratories to clinics [1–3]. Particular progress has been made in translational research of cytotoxic antimicrobial peptides (AMPs) [4,5]. Many AMPs which demonstrate toxicity against eukaryotic cells have been repurposed for applications in clinical oncology [6–13]. Major hurdles along this avenue have been, and still remain the unfavorable pharmacokinetic (PK) profiles and enhanced systemic toxicity of typical AMPs [11–14]. The latter is caused by unspecific cellular toxicity, which was identified as the primary reason for numerous failures of AMPs in advanced clinical development [1,3,5]. Therefore, much effort has been put into developing novel drug delivery

strategies, optimizing the pharmacological characteristics of AMPs and increasing their *in vivo* selectivity towards prokaryotic or malignant cells [1,15,16].

One of the promising novel approaches to alleviate excessive systemic toxicity and improve spatiotemporal selectivity of anticancer drug candidates is based on photocontrolled biologically active compounds (we call such compounds "lumobiotics"). Lumobiotics contain photoisomerisable fragments within their molecular framework. Hence, they may exist in at least two photoisomeric forms (photoforms), which are interconvertible by irradiation with light of different wavelengths (Fig. 1A). They are designed to be less bioactive and less toxic in one of the photoforms, while being more active and possessing the desired (high) level of biological activity when converted into the other

* Correspondence to: Igor V. Komarov, Institute of High Technologies, Taras Shevchenko National University of Kyiv, prosp. Hlushkova 4G, 03022 Kyiv, Ukraine

** Correspondence to: Anne S. Ulrich, Institute of Biological Interfaces (IBG-2), Karlsruhe Institute of Technology (KIT), P. O. Box 3640, 76021 Karlsruhe, Germany.

*** Correspondence to: Sergii Afonin, IBG-2 of KIT, P. O. Box 3640, 76021 Karlsruhe, Germany.

E-mail addresses: igor.komarov@knu.ua (I.V. Komarov), anne.ulrich@kit.edu (A.S. Ulrich), sergiy.afonin@kit.edu (S. Afonin).<https://doi.org/10.1016/j.jphotobiol.2022.112479>

Received 1 February 2022; Received in revised form 13 May 2022; Accepted 17 May 2022

Available online 24 May 2022

1011-1344/© 2022 The Authors. Published by Elsevier B.V. This is an open access article under the CC BY license (<http://creativecommons.org/licenses/by/4.0/>).

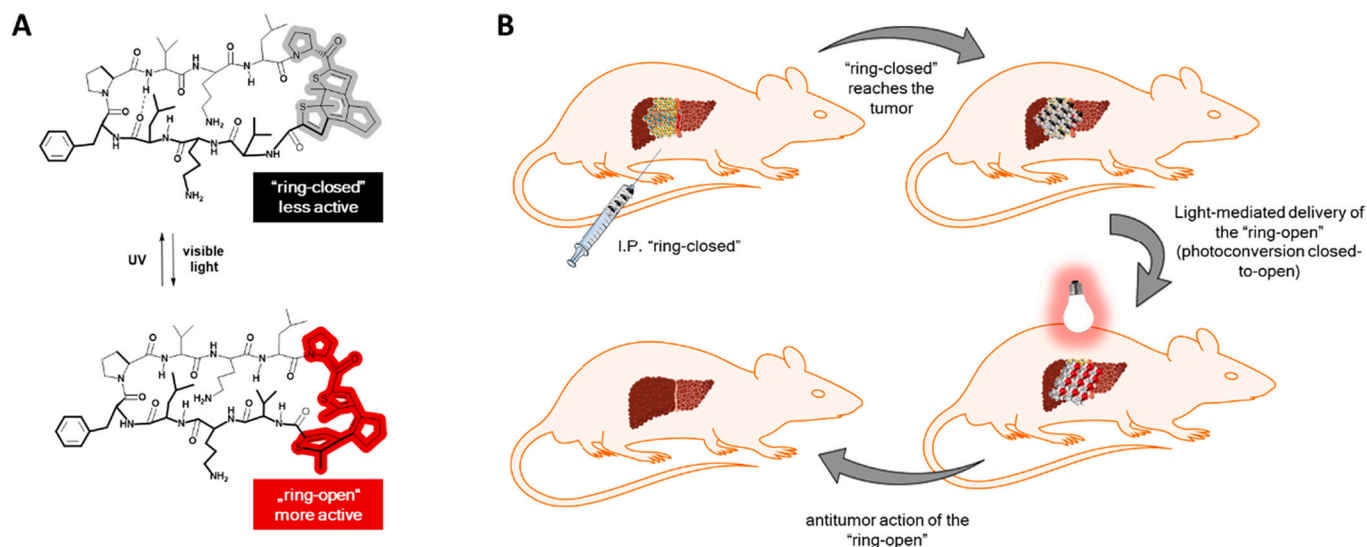


Fig. 1. (A) Photoswitchable cytotoxic peptide LMB002, a predecessor of LMB040 [25]. The peptide is a derivative of a natural cytolytic peptide gramicidin S, obtained by substituting two amino acid residues with a photoswitchable diarylethene fragment. The ring-closed diarylethene fragment within the less toxic photoform is shown in grey, and its ring-open photoform is highlighted by red in the more active photoisomer. (B) Illustration of the principle of the *in vivo* photo-mediated PCP delivery. The peptide is administered in the less toxic photoform and is activated (photoconverted) inside the body by external application of light [43]. (For interpretation of the references to colour in this figure legend, the reader is referred to the web version of this article.)

photoform. Photoisomerisable peptides have been intensively studied for many decades [17–23], and these efforts began finally to pay off in the medicinal chemistry field [24]. It has been postulated that such compounds, if administered in the less active forms and activated by light at the site of desired action (lesion, local inflammation, tumor, etc), might be safer drug candidates than the original, non-photocontrollable analogues due to decreased side toxicity. We have recently demonstrated *in vivo* that this is true for photocontrollable cytolytic peptides (PCPs) – derivatives of AMPs – in treating solid tumors [25,26]. Thus, *in vivo* generation of the bioactive form by applying light at the site of a tumor or any other desirable location can be regarded as a spatiotemporally controlled delivery of the therapeutic (Fig. 1B) that should enhance the translational potential of any such class of compounds. We identified previously, that the *in vivo* biodistribution of PCPs upon systemic administration could be an issue in itself: alternative photoforms may have different PK profiles and tissue accumulation patterns. We argue, however, that the “unfavorable” PK can offer advantages for drug development, at least in the case of PCPs. The dosage and the light application regiment could be optimised for using a cytotoxic PCP in those tissues where the less active, initially administered photoform accumulates most, and where the active form is retained for the longest time. This approach, called the “PK/PD-driven” (PD = pharmacodynamics) drug development, has been discussed in the literature for quite a while [27].

Therefore, the main objective of the present study was to use the prior knowledge of the *in vivo* biodistribution for two photoforms of the cytolytic lumobiotic LMB040. We carried out confirmatory PK and proceeded with the PD studies of antitumor efficacy, using a PK profile-suggested cancer murine model, analysed the outcome in more detail and compared it to a benchmark chemotherapeutic.

2. Materials and Methods

2.1. Materials

The diethylnitrosamine (DEN, >95% chemical purity as analysed by gas chromatography/mass spectrometry) was obtained from Sigma-Aldrich. Carbon tetrachloride was distilled before use. Reagents for the biochemical tests and pharmacokinetics study were from Sigma-

Aldrich or Fluka. The cytotoxic peptide LMB040 was synthesised using solid-phase peptide synthesis and prepared in its “ring-open” form, converted to the “ring-closed” form by irradiation with ultraviolet light (UV) and purified by preparative-scale high-performance liquid chromatography (HPLC) to >90% of chemical purity, as confirmed by analytical HPLC following the procedure described in [25]. The elemental composition of the LMB040 was confirmed by the mass spectrometry data recorded on a Bruker Autoflex III instrument using matrix-assisted laser induced desorption/ionization (MALDI) with TOF (time of flight) detection. The fetal bovine serum (FBS) was acquired from Gibco Life Technologies. The trypsin- ethylenediaminetetraacetic acid (EDTA), phenylmethylsulfonyl fluoride (PMSF), penicillin and streptomycin were obtained from Merck. Dulbecco’s modified Eagle’s medium (DMEM) and Roswell Park Memorial Institute (RPMI) media were obtained from Hyclone, Dulbecco’s phosphate-buffered saline (DPBS) was from Gibco.

2.2. Animals and Tumor Model

The study was carried out using outbred male Wistar rats, with an initial 110–130 g bodyweight, obtained from the animal facility of the Taras Shevchenko National University of Kyiv. All animals were acclimatised before the study. During the acclimatisation period (7 days), 4 animals were kept per cage. All animals were monitored daily. The animals had free access to a standardised rat-chow diet and boiled tap water during the acclimatisation period and the experiment. Other housing conditions were: hygienic level - good conventional; type of animal cages - stainless steel wire mesh; cage size - H x W x D: 50 × 58 × 30 cm; cleaning - by changing the bedding material twice a week; the number of animals per cage - 4 or less (in case of mortality); air exchange - 15–20 times/h; temperature - 22 ± 3 °C; relative humidity - 40–70%; lighting - 12 h light/dark cycles, except during treatment days, during which the animals were kept in darkness.

The study was approved by the Bioethics Commission of Educational and Scientific Centre “Institute of Biology” of the Taras Shevchenko National University of Kyiv. It was performed following the ethical standards of the European Convention for the Protection of Vertebrate Animals used for Experimental and Other Scientific Purposes (Strasbourg, 1986), OECD Guidance Document on the Recognition,

Assessment and Use of Clinical Signs as Humane End Points for Experimental Animals Used in Safety Evaluation (Series on Testing and Assessment, N°19, ENV/JM/MONO (2000)7, OECD, Paris, 2000) [50], and General Ethical Principles of Experiments using Animals (First National Congress of Bioethics, Kyiv, 2001).

DEN (200 mg/kg, dissolved in saline) was injected intraperitoneally to each animal. Two weeks afterwards, liver-damaging was initiated by administering CCl₄ (0.1 ml/100 g, diluted with sunflower oil, 1:1) subcutaneously two times per week, throughout 22 weeks.

2.3. Pharmacokinetic Study

Animals with hepatocellular carcinoma (HCC) generated as described above (20 weeks after the DEN administration) were used for the PK study. All animals fasted (16 h) before dosing. Five time points (5, 15, 60, 120 and 480 min) and intraperitoneal (IP) route of administration was set for this study. Three randomly selected animals were taken for each time point. LMB040 dose level was 2.5 mg/kg, the concentration in the injection formulation (saline) – 1.75 mg/ml, injected volume – 1.43 ml/kg. No obvious adverse effects were observed during this PK study. After decapitation of animals, blood collection was performed in BD Microtainers containing K₃EDTA. Blood samples were centrifuged for 10 min at 3000 rpm. The malignant and healthy liver tissue samples were collected and weighed. All samples were immediately processed, flash-frozen and stored at –70 °C until subsequent analysis. Solution of elacridar (400 ng/ml in water-methanol mixture 1:9, v/v) was used as internal standard (IS) to quantify LMB040 in plasma, liver and tumor samples. Plasma samples (40 µl) were mixed with 200 µl of IS solution. After mixing by pipetting and centrifuging for 4 min at 6000 rpm, 2 µl of each supernatant was used for the analysis. Liver and tumor samples (266–2649 mg) were homogenised with five parts of IS solution (1 w + 5 v) by stainless steel beads (1000 mg ± 50 mg) in the 1600 MiniG homogeniser for 60–120 s at 1200–1600 g. After this, the samples were centrifuged for 4 min at 14000 rpm, and 2 µl of each supernatant was used for the analysis.

Analyses of plasma samples were conducted by the Bioanalytical Laboratory at Enamine/Bienta. The concentration of LMB040 in the samples was determined using high-performance liquid chromatography/tandem mass spectrometry (HPLC-MS/MS). A Shimadzu HPLC system consisted of two isocratic LC-10ADvp pumps, a SIL-20 AC autosampler, an FCV-14AH sub-controller, and a DGU-14A degasser. Mass spectrometric analysis was performed using API 3000 (triple-quadrupole) instrument from AB Sciex with an electrospray (ESI) interface. The data acquisition and system control were performed using Analyst 1.6.3 (AB Sciex). The conditions for chromatographic separation were: column - YMC-Pack ODS-AQ (50 × 2 mm, 3 µm); column temperature - 30 °C; mobile phase A - acetonitrile:water:formic acid = 50:950:1; mobile phase B - acetonitrile:formic acid = 100:0:1; gradient - 0 min 15% B, 1.0 min 100% B, 1.2 min 100% B, 1.21 min 15% B, finish - 2.3 min; elution rate: 400 µl/min. A divert valve directed the flow to the detector from 1.4 to 1.9 min. MS/MS detection: scan type - positive MRM; ion source - turbo spray; ionization mode - ESI; nebulise gas flow - 15 l/min; curtain gas - 8 l/min; collision gas - 4 l/min; ion spray voltage - 5000 V; temperature - 400 °C. Calibration curves were obtained using a separate sample of LMB040 (ring-closed).

2.4. Treatment Efficacy Study

A group of normal healthy control animals (Group 1, *n* = 8) received only solvents (saline or sunflower oil) of the same volume, administration route and at the same time points as the experimental animals where HCC was generated. Four experimental animal groups (*n* = 8) bearing the HCC were assembled: (Group 2) HCC-bearing animals that received no treatment; (Group 3) 5-FU-treated HCC-bearing animals. The treatment in this group started from the 16th week. Clinically used fluorouracil (5-FU) formulation (Ebewe Pharma, 50 mg/ml of the active

substance) was injected into the animals from this group intraperitoneally, once per week at the dose of 15 mg/kg, until week 22; (Group 4) HCC-bearing animals which received LMB040 treatment combined with irradiation. The treatment started at the beginning of the 21st week. The compound was injected intraperitoneally (10 mg/kg in 0.5 ml of saline). After 4 h, the abdominal surface of the animals in the area of the liver projection was irradiated (~100 mW/cm², 15 min, red laser λ_{max} = 650 nm). After the LMB040 injection, the animals were kept in darkness for 48 h to avoid uncontrolled LMB040 activation, and the procedure (LMB040 injection, irradiation, darkness for 48 h) was repeated. After the second treatment, two animals of this group died in 1 and 3 h after the compound administration. Immediately before the death, these animals were inactive. We suggest that this happened due to idiosyncratic reactions; (Group 5) the animals of this group received the same treatment as Group 4, but without the irradiation. The experiment was terminated after 22 weeks since the last treatment by LMB040. Half of the animals from each group (*n* = 4 for Groups 1, 3, 5; *n* = 3 for groups 2, 4) were sacrificed by cervical dislocation after CO₂ anesthesia. In addition, when the signs of morbidity appeared (recumbent posture, labored breathing, unresponsiveness), the animals were sacrificed as well. The other half subjects were left for the survival test.

2.5. Necroscopy

The sacrificed animals were subjected to necropsy; the liver damage was assessed by two independent investigators using the following scoring system [28]: grade 0 = reddish-brown in colour, soft inconsistency, smooth surface, 1 = the liver was enlarged, friable, soft inconsistency, 2 = hepatic hyperemia, 3 = an enlarged liver with white focal areas of necrosis, 4 = an enlarged liver with white multifocal areas of necrosis, 5 = hepatic steatosis, the liver is soft, yellow, greasy, enlarged, 6 = the liver is mottled red with bile stained areas, of normal or increased size, 7 = contains visible nodules and fibrosis, 8 = micronodular, yellow, fatty, enlarged, 9 = macronodular, brown, non-greasy, shrunken, cirrhosis, 10 = explanted liver showing small single granules bodies, 11 = explanted liver showing large single granules bodies, 12 = explanted liver showing many small granules bodies, 13 = explanted liver showing many large granules bodies.

2.6. Microscopy

Sections from the dissected liver tissues were collected immediately after the sacrifice of the animals and fixed in 10% formalin buffered with 0.1 M phosphate buffer (pH 7.2). Each paraffin section (4 µm thickness) was prepared and stained with hematoxylin and eosin stains (H&E). The specimens were examined using the microscopes Olympus BX41 (Olympus Europe) and Primo Star (Carl Zeiss) at x100, x400 magnification. Digital cameras Olympus C-5050 Zoom and Sigeta LCMOS 9000 9.0MP (Sigeta) were used to obtain images. The following characteristics assessed overall liver tissue condition: typical/atypical histological structure of the tissue; shape and structure of the cells; colouration; level of an inflammatory process (infiltration of leukocytes of the stroma and parenchyma); fibrosis (abnormal connective tissue accumulation and incorporation in liver parenchyma); the state of the vascular bed. The level of fibrosis was assessed using the scoring system developed by Ishak [29,30]: 0 = no fibrosis, 1 = fibrous growths in some portal areas without or with short fibrous septa, 2 = fibrous growths in most portal areas without or with short fibrous septa, 3 = fibrous growths in most portal areas with single portal-portal septa, 4 = fibrous growths in most portal areas with pronounced portal-portal and portal-central septa, 5 = pronounced septa with single nodes, 6 = it is possible to establish cirrhosis.

2.7. Biochemistry

Immediately after the sacrifice of animals, the blood samples were

harvested from their femoral vein, left for 20 min to form a clot, after which the blood was centrifuged for 10 min at 3000 g. The serum obtained was subjected to the following tests, using standard sets of reagents: activity tests for the enzymes alanine aminotransferase (ALT), aspartate aminotransferase (AST), alkaline phosphatase (ALP), α -amylase (AML), lactate dehydrogenase (LDH); gamma-glutamyl-transpeptidase (GGT); urea, total (TB) and conjugated (CB) bilirubin, triglycerides, total protein levels were determined.

The livers were washed with saline containing 1 mM EDTA and 0.4 mM PMSF at pH 7.0 and flush-frozen at -70°C . After thawing, the samples were gently homogenised in saline containing 1 mM EDTA and 0.4 mM PMSF, filtered through 4 layers of gauze, centrifuged at 10000 g for 15 min to precipitate nuclei and mitochondria. The supernatant was collected and used for the analyses. The total protein content was determined by literature procedures [31].

Levels of malonic dialdehyde (MDA), carbonyl groups of proteins (PCG) and reduced glutathione (GSH), the activity of intracellular superoxide dismutase (SOD), catalase (CAT), glutathione peroxidase (GP) and total glutathione-S-transferase (GST) were determined spectrophotometrically and expressed per mg of protein.

The level of MDA was evaluated by reaction with thiobarbituric acid [32]. Chromogen absorption was determined at 532 nm, the content of lipid peroxidation products was expressed as MDA using the molar extinction coefficient of $1.56 \times 10^5 \text{ M}^{-1} \text{ cm}^{-1}$.

Protein carbonyls, a marker of global protein oxidation, were determined by the derivatising of the oxidised protein amino acid residues with dinitrophenylhydrazine [33]. The amount of stable 2,4-dinitrophenylhydrazone products was quantified at 370 nm, and the oxidised protein content was expressed as the amount of 2,4-dinitrophenylhydrazone using the molar extinction coefficient of $2.2 \cdot 10^4 \text{ M}^{-1} \text{ cm}^{-1}$.

The level of GSH was evaluated based on its ability to oxidise 5,5'-dithiobis- (2-nitrobenzoic acid) to form GSSG and 5-thio-2-nitrobenzoic acid (TNB), which has a maximum absorption at 412 nm [34].

Superoxide dismutase activity was evaluated by analysing its ability to inhibit the reduction of Nitro blue tetrazolium chloride (NBT) by riboflavin [35].

Formation of $\text{O}_2^{\cdot-}$ (and reduction of NBT to formazan) was initiated by illumination (bright sunlight) for 10 min, and the absorbance was determined at 540 nm. The unit of activity was considered to be the amount of enzyme required to inhibit NBT reduction by 1%.

Catalase activity was assessed by the reaction of H_2O_2 with molybdenum salts [36]. The reaction was initiated by adding 0.03% aqueous H_2O_2 solution to the analysed supernatant and was stopped after 10 min by adding 4% aqueous ammonium molybdate solution. Chromogen absorption was determined at 410 nm, and catalase activity was expressed as the rate of H_2O_2 decomposition using a molar extinction coefficient of $22.2 \text{ M}^{-1} \text{ cm}^{-1}$.

Glutathione peroxidase activity was assessed by determining the amount of unreacted GSH after adding to the reaction mixture and incubation with *t*-butyl hydroperoxide [37]. The amount of GSH was determined as described above. The total glutathione-S-transferase activity was assessed by measuring the binding of 1-chloro-2,4-dinitrobenzene to GSH, accompanied by an increase in absorption at 340 nm [38]. The molar extinction coefficient of $9600 \text{ M}^{-1} \text{ cm}^{-1}$ was used.

2.8. Survival

The Kaplan-Meier method was used for the analysis. After completion of treatment, the animals (half from each group, *i.e.* $n = 4$) were left for the survival test. No manipulations were performed with the animals during this period except weekly weighing.

2.9. Lymphoid Organ Index

The weights of lymphoid organs (thymus and spleen), their indices in

relation to the body weight of animals were evaluated as follows: rats were pre-weighed to control weight during tumor growth. After euthanasia, the animals were dissected, lymphoid organs (thymus and spleen) removed, and their weight determined. Indices of lymphoid organs in relation to the body weight of animals were calculated by the formula:

$$\text{Lymphoid organ index} = \text{Lymphoid organ weight} / \text{Animal weight}$$

2.10. Lymphoid Cells Isolation

Lymphocytes from the spleen and thymus of experimental animals were isolated from grinding tissue (had fixed weight) in a Potter homogeniser. Obtained cells were filtered through 70 μm filter and lymphocyte isolation was performed by centrifugation on the Histo-paque®-1077 density gradient (Sigma) at 400 g for 30 min. After that, lymphocytes were carefully selected with Pasteur pipette, twice washed in DPBS and counted in Goryaev chamber. Flow cytometry was used to determine the number of T-cells (CD3+ cells) in the lymphocyte cell suspension.

2.11. Flow Cytometry

Determination of the T-cell subpopulation was performed by flow cytometry using anti-rat mouse CD3 Monoclonal Antibody FITC (Invitrogen). The number of T-cells was determined from the total cell population preliminary counting them with a Goryaev chamber.

Cells at concentration 1×10^5 cells were used to prepare each sample (taking into account the weight of the lymphoid organ). Cell suspension was pelleted by centrifugation at 400 g for 5 min and washed with DPBS. To the cell suspension were added 10 μL of CD3 FITC Monoclonal Antibody and incubated for 20 min at 4°C (protected from sunlight). The samples were washed with 2 ml of DPBS for 10 min at 400 g. The pellet was fixed by adding 400 μl of 0.4% formalin solution in DPBS. Sample measurements were performed at least within 3 days on flow cytometer FACS Calibur (Becton Dickinson) with 488 nm argon and 635 nm diode lasers using CellQuest PRO software (Becton Dickinson). Number of T-cells was calculated as:

$$\text{Number of T-cells} = (\text{Lymphoid cell amount} \times \text{CD3+ cell percentage}) / \text{weight of lymphoid tissue specimen.}$$

2.12. Statistical Analysis

The data were checked for normality of distribution. ANOVA was used under conditions of the normal distribution; under conditions of abnormal distribution, the Mann-Whitney test was applied.

3. Results and Discussion

Our previous PK studies on a syngeneic heterotopic tumor mouse model [25] have demonstrated that a representative membranolytic PCP, LMB002 (Fig. 1A), possess different biodistribution profiles for its two thermostable photoforms. Upon intravenous bolus injection of the photoform mixture, the less active (ring-closed) isomer accumulated significantly in the kidneys, lung, heart and liver. Furthermore, it demonstrated the most prolonged residence in tumor tissues, whereas the activated (ring-open) form resided the longest time and accumulated mainly in the liver. The high blood supply could explain the specificity of the biodistribution of the more soluble ring-closed LMB002 to the accumulating organs. In contrast, the difference in the accumulation of the ring-open photoform could be attributed to the higher lipophilicity of the photoisomer. Taking into account the PK data, we hypothesize that membranolytic PCPs like LMB002 should be most efficient in treating malignancies either in kidneys (highest inactive form accumulation) or in the liver (longest active form residence). In order to verify this hypothesis, we carried out a PK study for an analogous PCP, LMB040 [39], on the advanced chemically induced hepatocellular carcinoma (HCC) in rats. Notably, treatment of the advanced HCC in

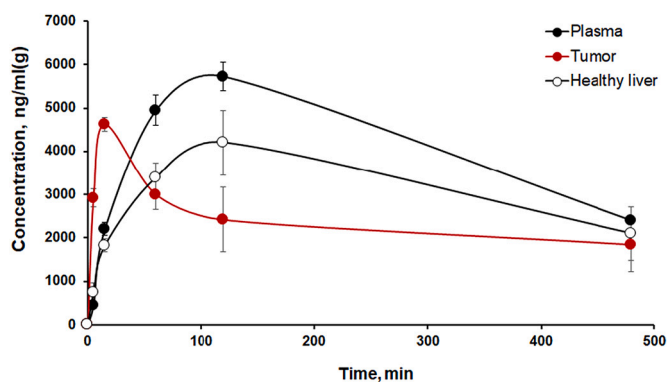


Fig. 2. Concentration-time curves for the ring-closed photoform in advanced HCC-bearing rats following IP administration (2.5 mg/kg).

humans by current treatment modalities has had rather limited success, and novel therapies are therefore of great interest [40–42].

To generate advanced HCC in rats for this study, we used a single-dose injection of the tissue-nonspecific genotoxicant, diethylnitrosamine (DEN), followed by repeated dosing of hepatic toxin carbon tetrachloride (CCl₄). This model is orthotopic and is characterised by the development of chronic inflammatory environmental characteristics of human HCC [44]. Furthermore, several publications have reported that the DEN/CCl₄-induced HCC generates tumors in rats that match by certain genetic characteristics the tumors in human HCC patients [45,46]. In addition, the use of immunocompetent animals provided a possibility to assess the immune response to the therapy, which is important for the design of future treatment strategies, especially in combination with currently popular immuno-oncologic approaches [42].

The PCP explored in this study, the photocontrollable gramicidin S analogue LMB040, is a cyclic molecule possessing a dithienylethene photoisomerisable fragment in the peptide backbone. The fragment undergoes reversible electrocyclic reaction upon irradiation with light; the UV light (~360 nm wavelength) creates the ring-closed photoform, while the red light (~650 nm) induces the formation of the ring-open photoform, as illustrated in Fig. 1A for LMB002. Both photoforms of LMB040 are sufficiently thermally stable and can be isolated, purified and studied separately. Furthermore, we have previously shown in a murine allograft model that a lumobiotic of this type can be administered in its ring-closed, less active form and then be activated directly in the tumor by irradiation with tissue-benign red light. In live animals, this activation has been efficient up to a depth of 1 cm [25,47]. Judging from the acute toxicity difference in mice between the two photoforms of five related PCP compounds (LD₅₀ of ring-closed vs. LD₅₀ of ring-open form), LMB040 is so far the safest lumobiotic in our hands [25].

According to our hypothesis, here we have first studied the PK of the less active LMB040 (ring-closed) in rats bearing advanced HCC (after 20 weeks from the initial DEN administration). The time-dependent LMB040 concentrations in blood plasma, healthy liver tissue, and tumor tissue are shown in Fig. 2, and selected PK parameters are summarised in Table 1.

The concentration of the less active form in liver tissue was found to

be almost as high as in plasma (liver and tumor tissue C_{max} are about 70–80% of the plasma value). It reached the highest healthy tissue concentration within approximately 2 h (T_{max}). We also note a difference with regard to the previous mouse PK data, where liver C_{max} for the LMB002 ring-closed photoform was about 30% of the plasma value. Correspondingly, AUC_{0–∞} values in the liver in the previous experiments were about twice smaller than the plasma values. All three AUC_{0–∞}, which we determined in the current experiment, are very similar. The elimination rate is comparable for both plasma and healthy liver tissue, and the residence time is sufficiently long (the half-life T_{1/2} is 287 and 360 min, correspondingly). However, the PK profile in HCC tissue is different: the concentration reached its maximum within less than half an hour, and thereafter receded much slower (T_{1/2} of 681 min).

Judging from the observed LMB040 ring-closed PK data, one might conclude that the ideal time point for the photoactivation of the lumobiotic would be at around 15 min after the IP administration, when the LMB040 concentration in tumor tissue is the highest; however, the illumination procedure itself takes time in the range of tens of minutes. Therefore, we selected a later timepoint to start the photoactivation in the therapeutic experiment. We argued that the intra-tissue drug activation/delivery in our experiment could be safely started once LMB040 is partly cleared from the plasma and healthy tissue, being at the same time almost constant and relatively high in the tumors and their surroundings (*i.e.* in 4–6 h).

We chose a well-known anticancer chemotherapeutic 5-fluorouracil (5-FU) as a benchmark in the therapeutic experiment. This pyrimidine-derived antimetabolite, which acts primarily through inhibition of thymidylate synthase, is a common treatment agent in established regimens against many carcinomas and sarcomas, including HCC. Its efficiency in treating human metastatic HCC has been demonstrated long ago [48]. However, the development of a 5-FU-resistant hepatocellular carcinoma cell lines has been reported to limit the therapy [49].

Schematically, the experiment design and experimental group designations (Groups 2–5) are illustrated in Fig. 3 (Group 1 was composed of the healthy untreated animals for the intact control).

The primary endpoint of the experiment was the median overall survival of the animals. Animals that were moribund or in a state of impending death [50] were euthanised to avoid unnecessary suffering, pain and distress, and these were counted as those who died during the study. In addition, we monitored the appearance and weight of all animals during the experiment. Finally, we measured their biochemical parameters reflecting the pathological processes in the liver of the sacrificed animals and characterised *post mortem* liver organs morphologically and histologically at week 24.

Animals appeared normal during the experiment, without any persisted signs of toxicity. Those few subjects that died during the study demonstrated body weight loss 1 or 2 weeks before death, and were observed possessing ungrounded fur. There was a substantial difference in the body weight between control healthy animals (Group 1) and HCC-bearing ones starting from the 20th week of the study, with no significant difference between Groups 2 to 5 (Fig. 4). We noted a tendency to decrease body weight in the 5-FU-treated HCC-bearing animals during the 5-FU interventions. After stopping the 5-FU administration, the body weight of the animals in the Group 3 seemed to stabilise. In the animals administered with LMB040 (Groups 4 and 5), we observed slight body

Table 1

Selected pharmacokinetic parameters^a for LMB040 (ring-closed) determined in advanced HCC-bearing rats following IP administration (2.5 mg/kg).

Tissue	T _{max} , min	C _{max} , ng/ml(g)	AUC _{0–t=480} , μg min/ml(g)	AUC _{0–∞} , μg min/ml(g)	T _{1/2} , min	K _{el} , min ⁻¹	MRT (last), min
plasma	120	5730	1960	2950	287	0.00241	188
healthy liver	120	4200	1490	2590	360	0.00192	200
tumor (liver)	15	4620	1150	2960	681	0.00102	202

^a T_{max} – time of maximum compound concentration; C_{max} – maximum concentration; AUC_{0–t=480} – area under the concentration vs time curve till the last time point measured; AUC_{0–∞} – area under the concentration vs time curve extrapolated to infinite time; T_{1/2} – half-life of the compound; K_{el} – elimination rate constant; MRT (last) – mean residence time from the time of dosing to the time of last measurable concentration;

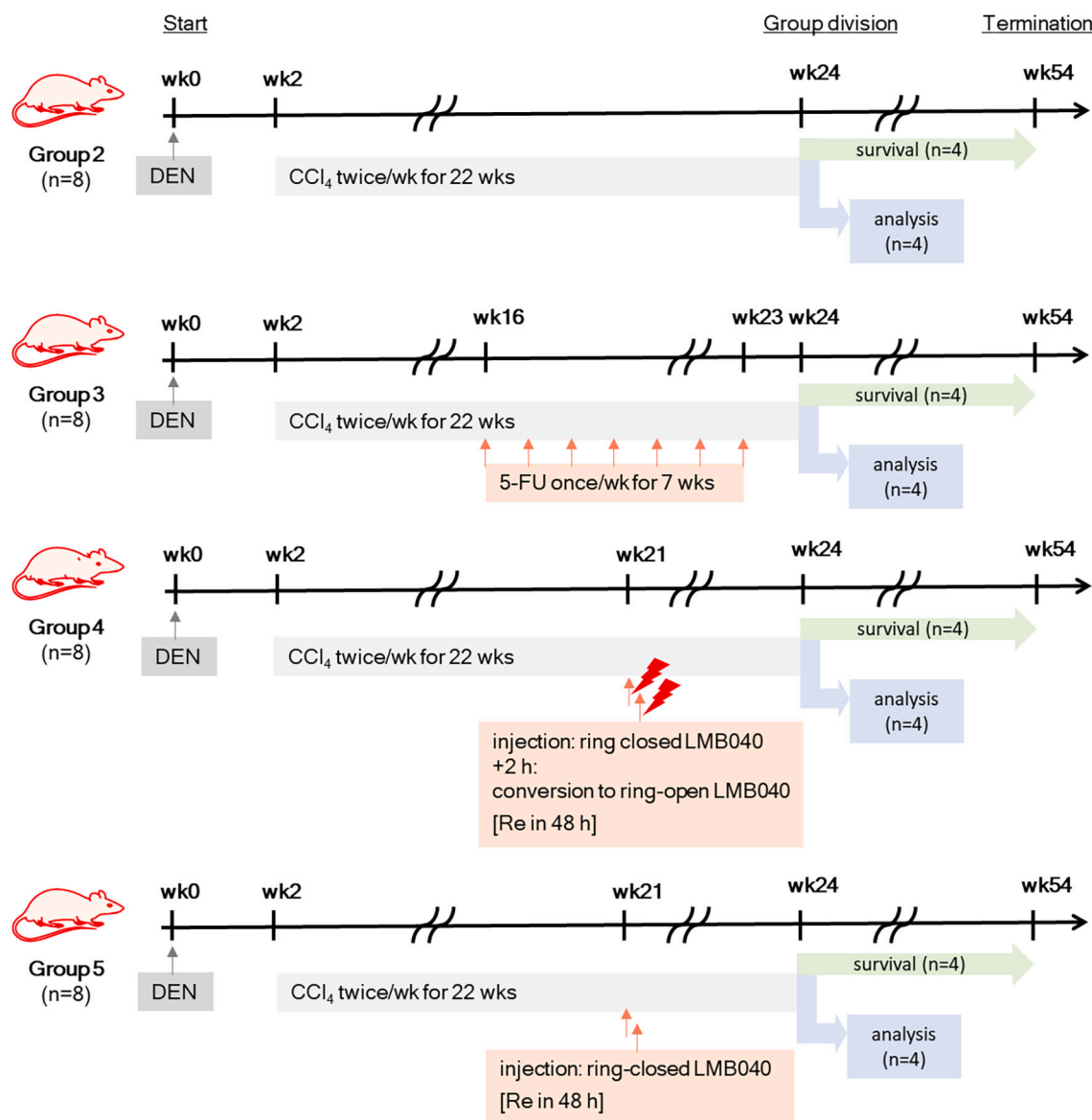


Fig. 3. Experimental group designations, tumor generation protocol (grey), schedule of the therapeutic experiment (peach/orange, lightning signs show the start of irradiation which lasted 15 min) carried out on the HCC-bearing male Wistar rats. Randomised separation of the subjects into two ($n = 4$) subgroups was planned at the 24th week. One subgroup was for necroscopy, histology, biochemistry (designated “analysis”, blue) and the second - for survival estimation (“survival”, green). Group 1 is a physiology control without HCC. (For interpretation of the references to colour in this figure legend, the reader is referred to the web version of this article.)

weight reduction at the week when interventions were performed, with subsequent body weight recovery (Fig. 4).

Representative images of the specimens for macroscopic and histology liver inspections are shown in Fig. 5 and Fig. 6. Results of the analysis of liver samples for total damage and for fibrosis (Ischak scoring) are listed in Table 2.

At the 24th week of the HCC generation, the livers of the untreated control animals (Group 2, $n = 3$) were characterised by multiple nodes of different sizes on the background of pronounced cirrhotic changes. The organs appeared dark, indicating blood stasis (Fig. 5B). Histology examination (Fig. 6B) revealed significant cirrhosis in the liver tissue (in the areas without visible signs of tumors). Large areas containing hypertrophied parenchymal cells with no cytoplasmic granulation were observed (presumably indicating focal nodular hyperplasia or hepatocellular adenoma) [51], as well as the areas of highly differentiated HCC cells. In addition, we noted dystrophic changes in the cytoplasm of some hepatocytes (eosinophilic or basophilic alteration), which often

contained enlarged nuclei with decondensed chromatin (signs of increased activity). Dilated blood capillaries were overfilled with blood, suggesting a portal hypertension.

The livers of animals treated with 5-FU for seven weeks under the condition of malignant liver degeneration (Group 3, $n = 4$, Fig. 5C) mainly corresponded to that of the untreated animals: multiple light nodules of different sizes on the background of cirrhosis were observed in both, light and dark liver tissue areas. In the histology analysis, significant inhibition of cirrhotic changes (by 35%) was evident: the portoportal septa were thin, the morphology of the liver between septa appeared intact, fibrotic outgrowths regions were often limited to portal areas without interconnections (Fig. 6E). However, eosinophilic alteration of some hepatocytes, signs of portal hypertension, and areas of focal nodular hyperplasia/adenoma were also observable in the specimens from this group.

The livers of animals treated with LMB040 ($n = 4$, Group 5) were of normal consistency, demonstrating typical (red-brown) colour, the

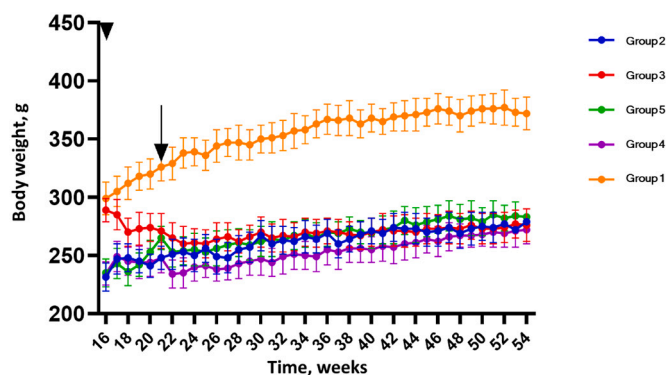


Fig. 4. Body weight dynamics from the 16th (when 5-FU treatment was started, indicated with an arrowhead) to the 54th week (the end of the study). The time point of LMB040 intervention (21st week) is indicated with an arrow.

organs possessed smooth edges, but individual tumor nodules were clearly seen on the inner surface of the lobes (Fig. 5D,E). Although macronodular cirrhosis was expressed in a single rat, the tumor nodules in this animal were observed only on the liver surface. Cirrhosis appeared mild according to histological analysis (Fig. 6F): porto-portal septa were not numerous, thin, and not always connective; the overall structure of the liver was not impaired, and significant suppression of fibrosis was observed compared with the untreated HCC-bearing animals (by 75%, Ischak score). However, liver hepatocytes eosinophilic/basophilic alteration remained, sometimes with clear focal nodular hyperplasia/adenoma.

The livers of the animals irradiated after the LMB040 administration ($n = 3$, Group 5) had uneven, bumpy surfaces, although the organs were of normal consistency and had smooth edges (Fig. 5F). Tumor nodules were of relatively small size; light spots (probably necrotic foci) were observed on the inner surface of the lobes and partially on the outer. Overall, the state of the liver appeared “worse” than in animals that were not exposed to irradiation. The symptoms of tissue cirrhosis were stronger manifested: porto-portal septa were more pronounced, and most appeared to be interconnected. Individual hepatocytes showed signs of eosinophilic/basophilic alteration and dystrophic changes. In addition, areas of focal nodular hyperplasia/adenoma were observed,

and there were clear foci of necrosis (Fig. 6H) in the connective tissue of the septa. Conclusions about the extent of the liver damage in different animal groups described above are corroborated by the quantitative indices shown in Table 2.

We measured selected hepatic biochemical indicators in the rat serum at week 24 to characterise liver and bile duct function in HCC-bearing animals and the effect of different treatment regimens. Namely, we measured the activity of alanine aminotransferase (ALT), aspartate aminotransferase (AST), alkaline phosphatase (ALP), α -amylase (AML), lactate dehydrogenase (LDH); gamma-glutamyl-transpeptidase (GGT). We also analysed the levels of urea, total and conjugated bilirubin, triglycerides, and total protein level. In addition, as the markers of the redox state of the liver, levels of malonic dialdehyde (MDA), carbonyl groups of proteins (PCG) and reduced glutathione (GSH), the activities of intracellular superoxide dismutase (SOD), catalase (CAT), glutathione peroxidase (GP) and total glutathione-S-transferase (GST) were determined in the liver samples. The obtained values are shown in Fig. 7 (serum analysis) and Table 3 (liver tissue analysis).

Compared to the intact (healthy) animals, the following changes in the serum of the HCC-bearing non-treated rats were statistically significant: increase in the amount of conjugated and total bilirubin (by 2.7 and 2.3 times, respectively), total protein (by 33%), AST activity (by 74%), GGT activity (by 4.8 times). However, other measured indicators changed insignificantly. The lack of observable changes in the values of ALT, ALP and LDH can be explained by the massive replacement of the liver parenchyma with connective and tumor tissue. The process could result in a smaller number of normally functioning hepatocytes and, accordingly, the total activity of the enzymes remained within normal limits instead of being elevated.

In the animals treated by 5-FU, the serum levels of conjugated and total bilirubin were significantly lower than in the HCC-bearing non-treated group (by 43% and 36%, respectively) but remained elevated relative to the healthy control (by 56% and 50%, respectively). Signs of oxidative stress were observed in the liver by increased levels of MDA and PCG (by 3.7 and 3.9 times, respectively). The activities of the antioxidant enzymes and the reduced glutathione content also increased (by 1.9–7.7 times), suggesting a secondary adaptation of tumors to oxidative stress, typical for HCC [52,53]. AST and GGT activities remained at the level of the untreated HCC group, and only AML activity

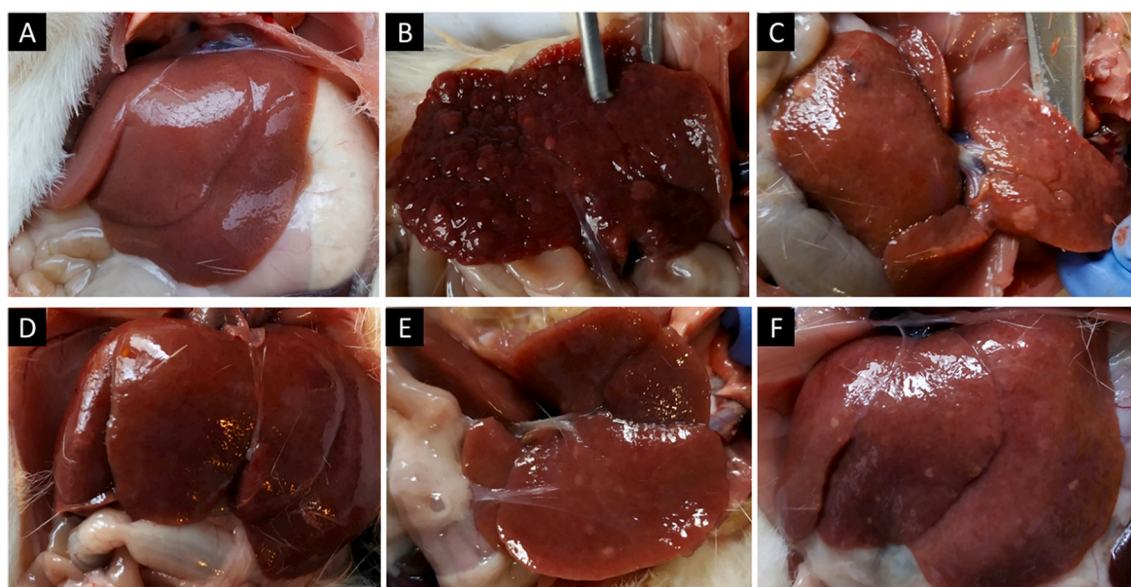


Fig. 5. Representative images of livers immediately after the necropsy. (A) Intact animals (Group 1); (B) HCC-bearing non-treated control animals (Group 2); (C) HCC-bearing animals treated with 5-FU (Group 3); (D, E) rats with HCC treated with LMB040 (Group 4); (E) inner liver lobes are shown; (F) HCC-bearing animals treated with LMB040 plus irradiation (Group 5).

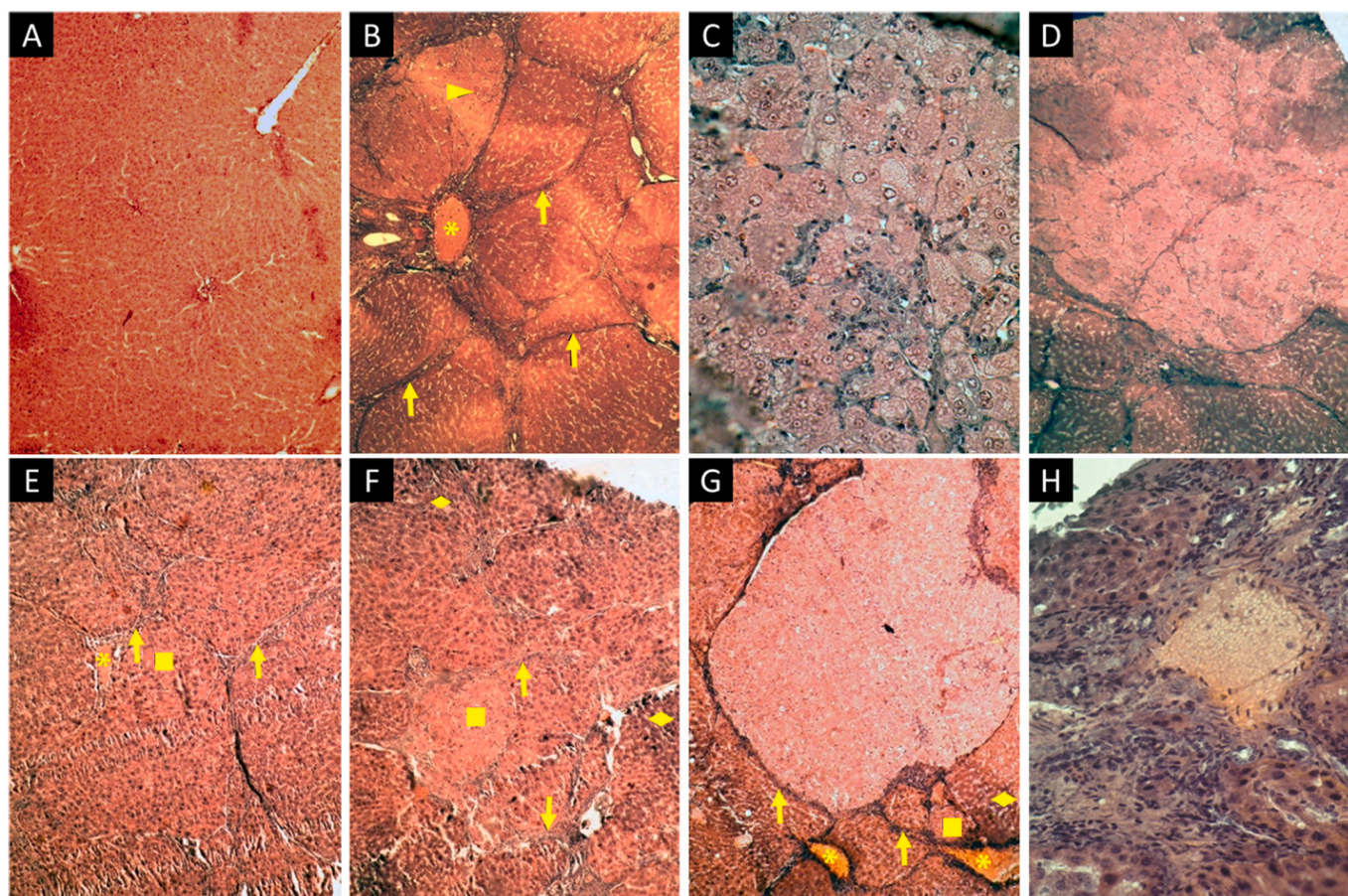


Fig. 6. Representative images of the histological examination of the liver tissue. (A) Intact animals (Group 1), $\times 100$; (B, C, D) HCC-bearing non-treated control (Group 2): (B) $\times 100$, fibrotic growth is visible, cirrhosis, (C) $\times 400$, highly differentiated hepatocellular carcinoma, (D) $\times 100$, area of focal nodular hyperplasia/hepatocellular adenoma; (E) 5-FU-treated animals (Group 3); (F) animals treated with LMB040 (Group 5), fibrous growth; (G, H) HCC-bearing rats treated with LMB040 plus irradiation (Group 4): (G) $\times 100$, area of focal nodular hyperplasia/hepatocellular adenoma; (H) $\times 400$, necrosis zone. Arrows mark porto-portal linking septa, asterisks mark blood vessel dilations, triangles indicate hepatocellular hypertrophy; hepatocytes eosinophilic alterations are marked by squares, hepatocytes basophilic alterations are marked by diamonds;

Table 2

Analysis of the rat liver damage (median [25;75] percentiles).

Indicator	Group 1 (n = 4)	Group 2 (n = 3)	Group 3 (n = 4)	Group 4 (n = 3)	Group 5 (n = 4)
Overall damage	0.0	11.0 [10.0;11.0]	10.5 [5.5;11.8]	10.0 [10.0;10.0]	10.0 [9.3;10.8]
Ischak scoring	0.0	5.0 [5.0;5.0]	3.3 [2.3;3.9] #p = 0.032	3.0 [2.0;3.0] #p = 0.046	1.3 [1.0;2.6] #p = 0.031

#p comparing to HCC-bearing non-treated control (p values are listed if $p < 0.1$).

decreased (by 55%). The content of peroxidation products of proteins and lipids decreased compared to untreated HCC-bearing animals (by 41% and 53%, respectively) but remained elevated relative to the healthy control (by 130% and 72%, respectively). The antioxidant activity of the enzymes remained similar, and the glutathione content reduced (36–89% compared to untreated HCC-bearing animals). The observed biomarker changes may indicate only a partial “normalization” of the redox balance in the liver, which probably reflects the overall “improvement” of liver condition. However, corroborating our necropsy results, the 5-FU therapy regiment does not appear to restore or compensate fibrotic degeneration to the full extend.

In the group treated with LMB040, the bilirubin levels decreased compared to untreated HCC-bearing animals (by 23–51%), although they remained elevated compared to the healthy control (by 34–68%). AST and GGT activities decreased to normal. The values of other indicators did not differ significantly from the HCC-bearing control. Signs

of oxidative stress in the liver persisted (increased MDA, PCG, SOD and GSH by 2–2.75 times compared with controls) but were less pronounced than in the untreated HCC-bearing animals (decrease by 21–65%). Accompanied with the decrease in the severity of cirrhotic changes and “normalization” of the functional state of the liver (beneficial treatment outcome is more pronounced than in the group treated with 5-FU), partial preservation of the signs of oxidative stress remained. Such overall therapy response may be due to the mechanism of LMB040 cytotoxic action, which we hypothesize is similar to the mechanism of action of the prototype cytolytic peptide gramicidin S. Namely, impaired cell membrane permeability (including mitochondrial), separation of respiration and oxidative phosphorylation, and induction of oxidative stress may explain the observed biochemical data, especially considering that the non-cancerous cells are less amenable to the direct compound action [36].

The serum and liver samples from the group treated with LMB040

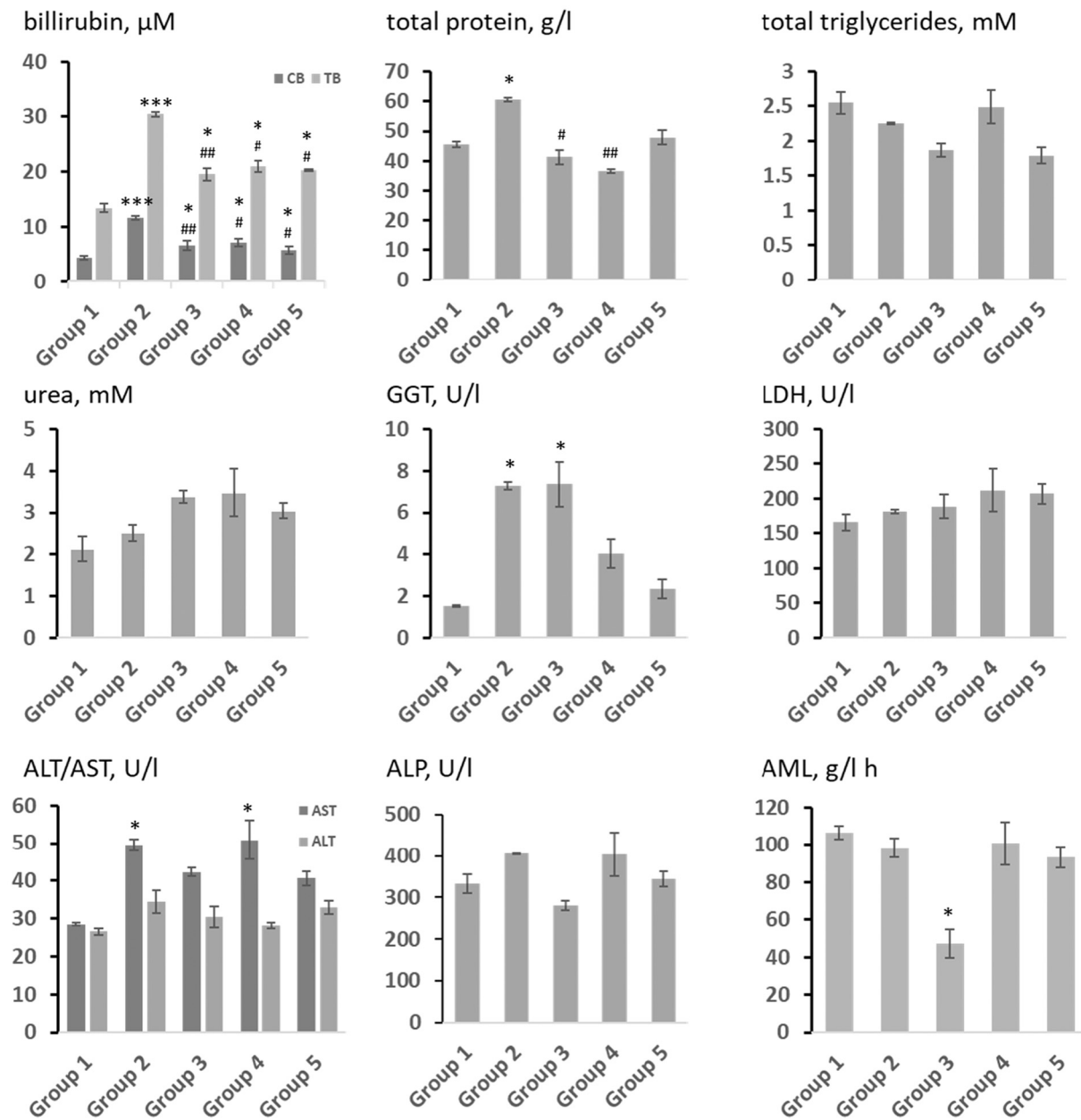


Fig. 7. Liver function biochemical data and additional health indicators, rat blood serum ($M \pm SEM$). *Comparing to the intact animals (p values < 0.1 : *** < 0.001 ; ** < 0.01 ; * < 0.1); # comparing to HCC-bearing non-treated control (p values < 0.1 : ### < 0.001 ; ## < 0.01 ; # < 0.1).

Table 3

Redox state characterization of rat liver (median [25;75] percentiles).

Indicator	Group 1	Group 2	Group 3	Group 4	Group 5
CAT, mol/mg prot	1.02 [0.76;1.28]	1.93 [1.02;1.99]	0.84 [0.72;1.06] # $p = 0.077$	0.14 [0.13;0.15] * $p = 0.053$	1.06 [0.95;1.72]
SOD, U/mg prot	34.26 [27.87;40.75]	266 [186.48;270] * $p = 0.025$	29.59 [22.79;34.09] # $p = 0.034$	31.11 [28.7;32.1] # $p = 0.05$	91.9 [65.42;126.27] * $p = 0.014$ # $p = 0.034$
GSH, nmol/mg prot	0.12 [0.09;0.18]	0.42 [0.16;0.5] * $p = 0.07$	0.11 [0.09;0.14] # $p = 0.034$	0.17 [0.09;0.18]	0.33 [0.2;0.63] * $p = 0.027$
GP, nmol/mg prot	0.96 [0.68;2.35]	2.6 [1.37;2.7]	0.88 [0.59;1.07] # $p = 0.034$	0.76 [0.42;0.84] # $p = 0.05$	1.74 [1.15;2.43]
GST, µmol/mg prot	110 [100.85;200.48]	256.5 [172.26;267.1]	165.41 [109.25;227.18]	17.03 [14.8;17.31] * $p = 0.025$ # $p = 0.05$	119.73 [114.38;393.59]
PCG, µmol/mg prot	148.5 [81.88;215.15]	578.5 [155.6;645.1]	341.1 [164.77;451.39]	145.34 [96.46;154.15]	392.83 [276.38;476.56] * $p = 0.027$
MDA, µmol/mg prot	0.23 [0.14;0.3]	0.84 [0.29;0.9] * $p = 0.072$	0.4 [0.26;0.58] * $p = 0.086$	0.3 [0.21;0.34]	0.48 [0.22;0.72] * $p = 0.086$

* comparing to the intact animals (p values are listed if $p < 0.1$); # comparing to HCC-bearing non-treated control (p values are listed if $p < 0.1$).

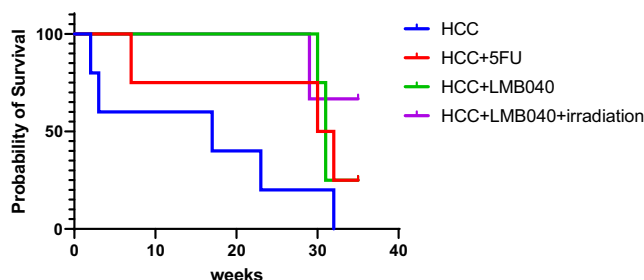


Fig. 8. The Kaplan-Meier survival curves for the studied experimental groups.

demonstrated a more pronounced overall normalization than LMB040 with irradiation. The serum bilirubin levels and GGT activity were lower than in the untreated HCC-bearing animals (by 33–68%) but higher than healthy controls (by 34–54%). Contrastingly, AST activity was maintained at the level of the HCC-bearing non-treated group. However, this apparent discrepancy could be explained by the lower prognostic ability of AST to the liver-only damage. Most importantly, signs of oxidative stress in the liver were virtually absent: levels of MDA, PCG, GSH, SOD, CAT and GP activity were indistinguishable from normal healthy controls (decreased by 26–88% compared with the HCC-bearing untreated group). Only net GST activity was significantly inhibited (by 85% compared to healthy control). Inhibition of GST activity is a proinflammatory factor and is observed in liver fibrosis and in the activated hepatic stellate cells [54]. Therefore, it is probable that the observed inhibition of the activity of this enzyme is a bare reflection of the more pronounced fibrous and cirrhotic changes in this group compared with the group treated with the LMB040 without irradiation, where other indicators of oxidative stress remained present.

Finally, the median overall survival determined in this study was the following (Fig. 8): HCC-bearing non-treated animals (Group 2) – 17 weeks; 5-FU treated animals (Group 3) – 30 weeks; animals treated with LMB040 followed by irradiation (Group 4) – 35 weeks, without irradiation (Group 5) – 31 weeks. Thus, LMB040 *per se* increases the survival of animals at the level of 5-FU (by 1.8 times), while LMB040 with irradiation – by 2.1 times, which confirms the validity of our experimental design.

There is a small but noticeable benefit of the light-induced PCP activation *in vivo* that formally satisfies our PK/PD-driven target tissue selection hypothesis, although the compound dosage and irradiation regimen should still be improved.

It is of great interest whether the treatment by the LMB040 causes immunogenic cell death [55] and subsequent activation of the immune system against the tumor antigens. An immune system activation and subsequent increase of the overall survival has been documented for solid tumors treated with other cytolytic peptides [56] and for oncolytic viruses. Our treatment caused an increase in the overall survival, but the

cooptation of the immune system to this effect remains an open question. To address it partially, we investigated the immune organs of the animals (spleen and thymus) in the LMB040-treated groups and compared them to the HCC-bearing control. The weight indices of the immune organs in the subjects collected for analysis at the 24th week were determined, and the number of the T-cells in each organ was estimated. The results are listed in Table 4. Since the weight indices of the organs were found identical within statistical limits throughout all animals, no hyperplasia could be attributed to the therapy. Therefore, the number of T-cells in the thymus of some animals in Group 4 (2 rats out of 3), which was more than an order of magnitude larger than in all other animals, could indicate the more active immune response system. We plan to investigate the possible involvement of the immune system in anticancer therapy by LMB040 and similar lumobiotics in the near future by means of white blood cell analysis.

4. Conclusions

We have confirmed the validity of the PK/PD-driven target selection for an anticancer cytolytic peptide LMB040 by demonstrating its effectiveness in a rat advanced HCC model. Through morphological and biochemical characterization, by observing differences in the pharmacodynamics of the drug in the two alternative photoisomeric states, we confirmed the possibility of a photo-mediated “delivery” of the biologically more active form lumobiotic LMB040 in rats. The PCP in the ring-closed photoform caused inhibition of fibrous degeneration of the liver, partial normalization of hepatic functional activity (more effective than the reference drug 5-FU). Nonetheless, the signs of oxidative stress persisted in the liver tissue for this treatment regimen. Upon photoconversion (*i.e.* delivery) of the PCP in the ring-open photoform, antifibrotic effects and restoration of the liver function were less pronounced. However, the signs of oxidative stress in the liver tissue were almost eliminated (effects similar to the reference drug 5-FU). The following order was established for the median overall survival: photoactivated LMB040 > non-photoactivated LMB040 > 5-FU. Activating the immune system upon photo-mediated intra-liver delivery of LMB040 deserves further investigations. Well-defined T-cell profiling and cytokine analysis in a broader set of tissues could further improve this photopharmacology approach as a novel modality of anticancer therapy.

CRedit authorship contribution statement

Igor V. Komarov: Conceptualization, Data curation, Formal analysis, Funding acquisition, Methodology, Project administration, Resources, Supervision, Validation, Visualization, Writing – original draft, Writing – review & editing. **Ganna Tolstanova:** Conceptualization, Formal analysis, Methodology, Project administration, Resources, Supervision. **Halyna Kuznietsova:** Data curation, Formal analysis, Investigation, Methodology, Validation, Visualization, Writing – review & editing. **Natalia Dziubenko:** Data curation, Formal analysis,

Table 4

Rat spleen and thymus parameters in the animals from Groups 2, 4 and 5, sacrificed at the 24th week of the study.

Animal	Group 2 (n = 3)			Group 4 (n = 3)			Group 5 (n = 4)			
	(i)	(ii)	(iii)	(i)	(ii)	(iii)	(i)	(ii)	(iii)	(iv)
<i>spleen parameters</i>										
Organ weight index, %	0.81	0.53	0.35	0.54	0.33	0.34	0.42	0.50	0.46	0.42
M ± SEM	0.56 ± 0.1			0.40 ± 0.07			0.45 ± 0.02			
Number of T-cells, 10 ⁶ /g	39	96	114	114	118	66	30	32	99	128
M ± SEM	82.9 ± 22.6			99.3 ± 16.7			72.2 ± 24.4			
<i>thymus parameters</i>										
Organ weight index, %	0.07	0.11	0.07	0.04	0.08	0.09	0.12	0.65	0.09	0.07
M ± SEM	0.08 ± 0.02			0.07 ± 0.02			0.23 ± 0.14			
Number of T-cells, 10 ⁶ /g	203.8	116.6	N/A	7500	4600	131.5	34	34	44	6.1
M ± SEM	160.2 ± 43.6			4077 ± 2143			29.5 ± 8.2			

Investigation, Resources, Validation, Visualization, Writing – review & editing. **Petro I. Yanchuk**: Data curation, Investigation, Validation. **Lydia Y. Shtanova**: Investigation. **Stanislav P. Veselsky**: Investigation, Writing – review & editing. **Liudmyla V. Garmanchuk**: Conceptualization, Formal analysis, Investigation, Methodology, Supervision, Validation, Visualization, Writing – review & editing. **Nataliia Khranovska**: Data curation, Formal analysis, Methodology, Supervision, Validation. **Oleksandr Gorbach**: Data curation, Investigation. **Taisa Dovbynchuk**: Investigation. **Petro Borysko**: Data curation, Formal analysis, Investigation, Methodology, Project administration, Supervision, Validation, Visualization. **Oleg Babii**: Conceptualization, Formal analysis, Funding acquisition, Investigation, Methodology, Project administration, Supervision, Validation. **Tim Schober**: Conceptualization, Data curation, Formal analysis, Funding acquisition, Investigation, Methodology, Validation. **Anne S. Ulrich**: Funding acquisition, Resources, Writing – review & editing. **Sergii Afonin**: Conceptualization, Data curation, Formal analysis, Funding acquisition, Methodology, Project administration, Supervision, Validation, Visualization, Writing – original draft, Writing – review & editing.

Declaration of Competing Interest

IVK, OB, SA and ASU are inventors on the issued patent family: “Peptidomimetics possessing photocontrolled biological activity” (WO2014127919 [A1], EP2958934 [B1], US9481712 [B2], UA113685 [C2]). IVK, OB, TS and SA are founders and shareholders of Lumobiotics GmbH. IVK is a scientific advisor, HK and PB are employees of Enamine LLC. The authors have no other relevant affiliations or financial involvement with any organization or entity with a financial interest in or financial conflict with the subject matter or materials discussed in the manuscript apart from those disclosed.

Acknowledgements

The authors acknowledge EU funding by the H2020-MSCA-RISE program through PELICO (#690973) and ALISE (#101007256) projects. This work was supported by the DFG-GRK 2039 (SA, TS and ASU), the NACIP program of the Helmholtz Society (SA and ASU), and the VIP+ of the BMBF (OB and ASU). We acknowledge support by the KIT-Publication Fund of the Karlsruhe Institute of Technology. The authors thank all brave defenders of Ukraine that made finalizing this publication possible.

References

- [1] M. Muttenthaler, G.F. King, D.J. Adams, P.F. Alewood, Trends in peptide drug discovery, *Nat. Rev. Drug Discov.* 20 (2021) 309–325, <https://doi.org/10.1038/s41573-020-00135-8>.
- [2] M.A. Abdalla, L.J. McGaw, Natural cyclic peptides as an attractive modality for therapeutics: a mini review, *Molecules* 23 (2018) 2080, <https://doi.org/10.3390/molecules23082080>.
- [3] A. Henninot, J.C. Collins, J.M. Nuss, The current state of peptide drug discovery: back to the future? *J. Med. Chem.* 61 (2018) 1382–1414, <https://doi.org/10.1021/acs.jmedchem.7b00318>.
- [4] Y. Huan, Q. Kong, H. Mou, H. Yi, Antimicrobial peptides: classification, design, application and research progress in multiple fields, *Front. Microbiol.* 11 (2020) 2559, <https://doi.org/10.3389/fmicb.2020.582779>.
- [5] A. Boto, J.M. Pérez de la Lastra, C.C. González, The road from host-defense peptides to a new generation of antimicrobial drugs, *Molecules* 23 (2018) 311, <https://doi.org/10.3390/molecules23020311>.
- [6] M.R. Felício, O.N. Silva, S. Gonçalves, N.C. Santos, O.L. Franco, Peptides with dual antimicrobial and anticancer activities, *Front. Chem.* 5 (2017) 5, <https://doi.org/10.3389/fchem.2017.00005>.
- [7] G. Gabernet, A.T. Müller, J.A. Hiss, G. Schneider, Membranolytic anticancer peptides, *MedChemComm* 7 (2016) 2232–2245, <https://doi.org/10.1039/C6MD00376A>.
- [8] K.S. Mohd, S. Dharmaraj, A. Azemin, M.A.K. Hassan, A review of potential anticancers from antimicrobial peptides, *Int J Pharm Pharm Sci* 7 (2015) 19–26.
- [9] Y.F. Xiao, M.M. Jie, B.S. Li, C.J. Hu, R. Xie, B. Tang, S.M. Yang, Peptide-based treatment: a promising cancer therapy, *J Immunol Res* 2015 (2015), 761820, <https://doi.org/10.1155/2015/761820>.

- [10] D. Gaspar, A.S. Veiga, M.A. Castanho, From antimicrobial to anticancer peptides. A review, *Front. Microbiol.* 4 (2013) 294, <https://doi.org/10.3389/fmicb.2013.00294>.
- [11] S. Riedl, D. Zweytick, K. Lohner, Membrane-active host defense peptides—challenges and perspectives for the development of novel anticancer drugs, *Chem. Phys. Lipids* 164 (2011) 766–781, <https://doi.org/10.1016/j.chemphyslip.2011.09.004>.
- [12] D.W. Hoskin, A. Ramamoorthy, Studies on anticancer activities of antimicrobial peptides, *BBA-Biomembranes* 1778 (2008) 357–375, <https://doi.org/10.1016/j.bbame.2007.11.008>.
- [13] J.S. Mader, D.W. Hoskin, Cationic antimicrobial peptides as novel cytotoxic agents for cancer treatment, *Expert Opin. Investig. Drugs* 15 (2006) 933–946, <https://doi.org/10.1517/13543784.15.8.933>.
- [14] R.E. Hancock, H.G. Sahl, Antimicrobial and host-defense peptides as new anti-infective therapeutic strategies, *Nat. Biotechnol.* 24 (2006) 1551–1557, <https://doi.org/10.1038/nbt1267>.
- [15] S. Er, U. Larai, R. Arshad, S. Sargazi, A. Rahdar, S. Pandey, A.M. Díez-Pascual, Amino acids, peptides, and proteins: implications for nanotechnological applications in biosensing and drug/gene delivery, *Nanomaterials* 11 (2021) 3002, <https://doi.org/10.3390/nano11113002>.
- [16] C.K. Wang, D.J. Craik, Designing macrocyclic disulfide-rich peptides for biotechnological applications, *Nat. Chem. Biol.* 14 (2018) 417–427, <https://doi.org/10.1038/s41589-018-0039-y>.
- [17] V. Peddie, A.D. Abell, Photocontrol of peptide secondary structure through non-azobenzene photoswitches, *J Photochem Photobiol C: Photochem Rev* 40 (2019) 1–20, <https://doi.org/10.1016/j.jphotochemrev.2019.05.001>.
- [18] S. Kitzig, M. Thilemann, T. Cordes, K. Rück-Braun, Light-switchable peptides with a hemithioindigo unit: peptide design, photochromism, and optical spectroscopy, *ChemPhysChem* 17 (2016) 1252–1263, <https://doi.org/10.1002/cphc.201501050>.
- [19] R.J. Mart, R.K. Allemann, Azobenzene photocontrol of peptides and proteins, *Chem. Commun.* 52 (2016) 12262–12277, <https://doi.org/10.1039/c6cc04004g>.
- [20] W. Szymanski, J.M. Beierle, H.A. Kistemaker, W.A. Velema, B.L. Feringa, Reversible photocontrol of biological systems by the incorporation of molecular photoswitches, *Chem. Rev.* 113 (2013) 6114–6178, <https://doi.org/10.1021/cr300179f>.
- [21] C. Renner, L. Moroder, Azobenzene as conformational switch in model peptides, *ChemBioChem* 7 (2006) 868–878, <https://doi.org/10.1002/cbic.200500531>.
- [22] C. Renner, U. Kusebauch, M. Löweneck, A.G. Millbradt, L. Moroder, Azobenzene as photoresponsive switch in cyclic peptides, *J. Pept. Res.* 65 (1) (2005) 4–14, <https://doi.org/10.1111/j.1399-3011.2004.00203.x>.
- [23] O. Pieroni, A. Fissi, N. Angelini, F. Lenci, Photoresponsive polypeptides, *Acc. Chem. Res.* 34 (2001) 9–17, <https://doi.org/10.1021/ar990141+>.
- [24] L. Albert, O. Vázquez, Photoswitchable peptides for spatiotemporal control of biological functions, *Chem. Commun.* 55 (2019) 10192–10213, <https://doi.org/10.1039/C9CC03346G>.
- [25] O. Babii, S. Afonin, T. Schober, L.V. Garmanchuk, L.I. Ostapchenko, V. Yurchenko, S. Zozulya, O. Tarasov, I. Pishel, A.S. Ulrich, I.V. Komarov, Peptide drugs for photopharmacology: how much of a safety advantage can be gained by photocontrol? *Future Drug Discov.* 2 (2020) FDD28, <https://doi.org/10.4155/fdd-2019-00033>.
- [26] S. Afonin, O. Babii, A. Reuter, V. Middel, M. Takamiya, U. Strähle, I.V. Komarov, A. S. Ulrich, Light-controllable dithienylethene-modified cyclic peptides: Photoswitching the *in vivo* toxicity in zebrafish embryos, *Beilstein J. Org. Chem.* 16 (2020) 39–49, <https://doi.org/10.3762/bjoc.16.6>.
- [27] J.M. Gallo, Pharmacokinetic/pharmacodynamic-driven drug development, *Mt Sinai J. Med.* 77 (2010) 381–388, <https://doi.org/10.1002/msj.20193>.
- [28] X.Q. Liu, X.J. Hu, H.X. Xu, X.Y. Zeng, Xiaochaihu decoction attenuates the vicious circle between the oxidative stress and the ALP inactivation through LPS-catecholamines interactions in gut, liver and brain during CCI 4+ ethanol-induced mouse HCC, *BMC Complement. Altern. Med.* 13 (2013) 375, <https://doi.org/10.1186/1472-6882-13-375>.
- [29] K.G. Ishak, Chronic hepatitis: morphology and nomenclature, *Mod. Pathol.* 7 (1994) 690–713.
- [30] B.C. Fuchs, Y. Hoshida, T. Fujii, L. Wei, S. Yamada, G.Y. Lauwers, C.M. McGinn, D. K. DePeralta, X. Chen, T. Kuroda, M. Lanuti, A.D. Schmitt, S. Gupta, A. Crenshaw, R. Onofrio, B. Taylor, W. Winckler, N. Bardeesy, P. Caravan, T.R. Golub, K. K. Tanabe, Epidermal growth factor receptor inhibition attenuates liver fibrosis and development of hepatocellular carcinoma, *Hepatology* 59 (2014) 1577–1590, <https://doi.org/10.1002/hep.26898>.
- [31] O. Lowry, N. Rosenbrough, A. Farr, R. Randall, Protein measurement with the Folin phenol reagent, *J. Biol. Chem.* 193 (1951) 265–275, [https://doi.org/10.1016/S0021-9258\(19\)52451-6](https://doi.org/10.1016/S0021-9258(19)52451-6).
- [32] N. Tuzokzan, H. Erdamar, I. Seven, Measurement of total malondialdehyde in plasma and tissues by high-performance liquid chromatography and thiobarbituric acid assay, *Firat. Tip Dergisi* 11 (2006) 88–92.
- [33] D. Weber, M.J. Davies, T. Grune, Determination of protein carbonyls in plasma, cell extracts, tissue homogenates, isolated proteins: focus on sample preparation and derivatization conditions, *Redox Biol.* 5 (2015) 367–380, <https://doi.org/10.1016/j.redox.2015.06.005>.
- [34] T.E. Tipple, L.K. Rogers, Methods for the determination of plasma or tissue glutathione levels, *Methods Mol. Biol.* 889 (2012) 315–324, https://doi.org/10.1007/978-1-61779-867-2_20.
- [35] G. Salbitani, V. Vona, C. Bottone, M. Petriccione, S. Carfagna, Sulfur deprivation results in oxidative perturbation in *Chlorella sorokiniana* (211/8k), *Plant Cell Physiol.* 56 (2015) 897–905, <https://doi.org/10.1093/pcp/pcv015>.

- [36] L. Góth, A simple method for determination of serum catalase activity and revision of reference range, *Clin. Chim. Acta* 196 (1991) 143–151, [https://doi.org/10.1016/0009-8981\(91\)90067-m](https://doi.org/10.1016/0009-8981(91)90067-m).
- [37] B. Faraji, H.K. Kang, J.L. Valentine, Methods compared for determining glutathione peroxidase activity in blood, *Clin. Chem.* 33 (1987) 539–543.
- [38] L.O. Nilsson, A. Gustafsson, B. Mannervik, Redesign of substrate-selectivity determining modules of glutathione transferase A1–1 installs high catalytic efficiency with toxic alkenal products of lipid peroxidation, *Proc. Natl. Acad. Sci. U. S. A.* 97 (2000) 9408–9412, <https://doi.org/10.1073/pnas.150084897>.
- [39] O. Babii, S. Afonin, A.Y. Ishchenko, T. Schober, A.O. Negelia, G.M. Tolstanova, L. V. Garmanchuk, L.I. Ostapchenko, I.V. Komarov, A.S. Ulrich, Structure–activity relationships of photoswitchable diarylethene-based β -hairpin peptides as membranolytic antimicrobial and anticancer agents, *J. Med. Chem.* 61 (2018) 10793–10813, <https://doi.org/10.1021/acs.jmedchem.8b01428>.
- [40] A. Likhitsup, N. Razumilava, N.D. Parikh, Treatment for advanced hepatocellular carcinoma: current standard and the future, *Clin. Liver. Dis. (Hoboken)* 13 (2019) 13–19, <https://doi.org/10.1002/cld.782>.
- [41] Z. Walther, D. Jain, Molecular pathology of hepatic neoplasms: classification and clinical significance, *Pathol. Res. Int.* 2011 (2011), 403929, <https://doi.org/10.4061/2011/403929>.
- [42] M.P. Johnston, S.I. Khakoo, Immunotherapy for hepatocellular carcinoma: current and future, *World J. Gastroenterol.* 25 (2019) 2977–2989, <https://doi.org/10.3748/wjg.v25.i24.2977>.
- [43] This image contains Servier Medical Art elements licensed under a Creative Commons Attribution 3.0 Unported License. <https://smart.servier.com>, 2021 (accessed on 15.12.2021).
- [44] Z.M. Jilkova, K. Kurma, T. Decaens, Animal models of hepatocellular carcinoma: the role of immune system and tumor microenvironment, *Cancers (Basel)* 11 (2019) 1487, <https://doi.org/10.3390/cancers11101487>.
- [45] P. Newell, A. Villanueva, S.L. Friedman, K. Koike, J.M. Llovet, Experimental models of hepatocellular carcinoma, *J. Hepatol.* 48 (2008) 858–879, <https://doi.org/10.1016/j.jhep.2008.01.008>.
- [46] E. Mansour, A. Zaky, N. Abdelmoneim, A.R. Bassiouny, Reversal of EMT by regulation of miR-200c through treatment of metformin and resveratrol in DEN-induced rat HCC, *Int. J. Adv. Res.* 4 (2016) 1274–1284.
- [47] O. Babii, S. Afonin, L.V. Garmanchuk, V.V. Nikulina, T.V. Nikolaienko, O. V. Storozhuk, D.V. Shelest, O.I. Dasyukevich, L.I. Ostapchenko, V. Iurchenko, S. Zozulya, A.S. Ulrich, I.V. Komarov, Direct photocontrol of peptidomimetics: an alternative to oxygen-dependent photodynamic cancer therapy, *Angew. Chem. Int. Ed. Eng.* 55 (2016) 5493–5496, <https://doi.org/10.1002/anie.201600506>.
- [48] M. Ikeda, T. Okusaka, H. Ueno, Y. Takezako, C. Morizane, A phase II trial of continuous infusion of 5-fluorouracil, mitoxantrone, and cisplatin for metastatic hepatocellular carcinoma, *Cancer* 103 (2005) 756–762, <https://doi.org/10.1002/cncr.20841>.
- [49] K. Uchibori, A. Kasamatsu, M. Sunaga, S. Yokota, T. Sakurada, E. Kobayashi, M. Yoshikawa, K. Uzava, S. Ueda, H. Tanzawa, N. Sato, Establishment and characterization of two 5-fluorouracil-resistant hepatocellular carcinoma cell lines, *Int. J. Oncol.* 40 (2012) 1005–1010, <https://doi.org/10.3892/ijo.2011.1300>.
- [50] OECD Guidance Document on the Recognition, Assessment and Use of Clinical Signs as Humane End Points for Experimental Animals Used in Safety Evaluation, *Series on Testing and Assessment, N°19, ENV/JM/MONO (2000)7*, OECD, Paris, 2000.
- [51] Z. Walther, D. Jain, Molecular pathology of hepatic neoplasms: classification and clinical significance, *Pathol. Res. Int.* 2011 (2011), 403929, <https://doi.org/10.4061/2011/403929>.
- [52] S.B. Cheng, H.T. Liu, S.Y. Chen, P.T. Lin, C.Y. Lai, Y.C. Huang, Changes of oxidative stress, glutathione, and its dependent antioxidant enzyme activities in patients with hepatocellular carcinoma before and after tumor resection, *PLoS One* 12 (2017), e0170016, <https://doi.org/10.1371/journal.pone.0170016>.
- [53] S.M. Tsai, S.K. Lin, K.T. Lee, J.K. Hsiao, J.C. Huang, S.H. Wu, H. Ma, S.H. Wu, L. Y. Tsai, Evaluation of redox statuses in patients with hepatitis B virus-associated hepatocellular carcinoma, *Ann. Clin. Biochem.* 46 (2009) 394–400, <https://doi.org/10.1258/acb.2009.009029>.
- [54] H. Chen, Q. Gan, C. Yang, X. Peng, J. Qin, S. Qui, Y. Jiang, S. Tuu, Y. He, S. Li, H. Yang, L. Tao, Y. Peng, A novel role of glutathione S-transferase A3 in inhibiting hepatic stellate cell activation and rat hepatic fibrosis, *J. Transl. Med.* 17 (2019) 280, <https://doi.org/10.1186/s12967-019-2027-8>.
- [55] L. Galluzzi, I. Vitale, S. Warren, S. Adjemian, P. Agostinis, A.B. Martinez, T. A. Chan, G. Coukos, S. Demaria, E. Deutsch, D. Draganov, R.L. Edelson, S. C. Formenti, J. Fucikova, L. Gabriele, U.S. Gaipl, S.R. Gameiro, A.D. Garg, E. Golden, J. Han, K.J. Harrington, A. Hemminki, J.W. Hodge, D.M.S. Hossain, T. Illidge, M. Karin, H.L. Kaufman, O. Keep, G. Kroemer, J.J. Lasarte, S. Loi, M. T. Lotze, G. Manic, T. Merghoub, A.A. Melcher, K.L. Mossman, F. Prosper, Ø. Rekdal, M. Rescigno, C. Riganti, A. Sistigu, M.J. Smyth, R. Spisek, J. Stagg, B. E. Strauss, D. Tang, K. Tatsuno, S.W. van Gool, P. Vandenabeele, T. Yamazaki, D. Zamarin, L. Zitvogel, A. Cesano, F.M. Marincola, Consensus guidelines for the definition, detection and interpretation of immunogenic cell death, *J. Immunother. Cancer* 8 (2020), e000337, <https://doi.org/10.1136/jitc-2019-000337>.
- [56] J. Nestvold, M.Y. Wang, K.A. Camilio, S. Zinöcker, T.E. Tjelle, A. Lindberg, B. E. Haug, G. Kvalheim, Sveinbjørnsson, : & Rekdal, Ø., Oncolytic peptide LTX-315 induces an immune-mediated abscopal effect in a rat sarcoma model, *Oncoimmunology* 6 (2017), e1338236, <https://doi.org/10.1080/2162402X.2017.1338236>.